

# Divide and Merge: Motion and Semantic Learning in End-to-End Autonomous Driving

Yinzhe Shen<sup>1</sup> Ömer Şahin Taş<sup>1,2</sup> Kaiwen Wang<sup>1</sup> Royden Wagner<sup>1</sup> Christoph Stiller<sup>1,2</sup>

<sup>1</sup>Karlsruhe Institute of Technology (KIT) <sup>2</sup>FZI Research Center for Information Technology

## Abstract

Perceiving the environment and its changes over time corresponds to two fundamental yet heterogeneous types of information: semantics and motion. Previous end-to-end autonomous driving works represent both types of information in a single feature vector. However, including motion tasks, such as prediction and planning, always impairs detection and tracking performance, a phenomenon known as negative transfer in multi-task learning. To address this issue, we propose Neural-Bayes motion decoding, a novel parallel detection, tracking, and prediction method separating semantic and motion learning, similar to the Bayes filter. Specifically, we employ a set of learned motion queries that operate in parallel with the detection and tracking queries, sharing a unified set of recursively updated reference points. Moreover, we employ interactive semantic decoding to enhance information exchange in semantic tasks, promoting positive transfer. Experiments on the nuScenes dataset show improvements of 5% in detection and 11% in tracking. Our method achieves state-of-the-art collision rates in open-loop planning evaluation without any modifications to the planning module.

## 1. Introduction

Modular end-to-end (E2E) autonomous driving (AD) is gaining attention as it combines the advantages of traditional pipeline methods and strict E2E approaches. The modular E2E framework essentially represents a multi-task learning challenge. It is anticipated that the various tasks complement each other [12], collectively enhancing the overall system performance. However, a poorly designed multi-task learning structure could not only fail to facilitate mutual learning but also adversely affect individual tasks, a phenomenon known as negative transfer [12]. The prevalent modular E2E approaches [21, 22, 55] typically employ a sequential structure (Fig. 1a). This structure aligns with human tendencies when performing driving tasks and has demonstrated promising planning performance. However,

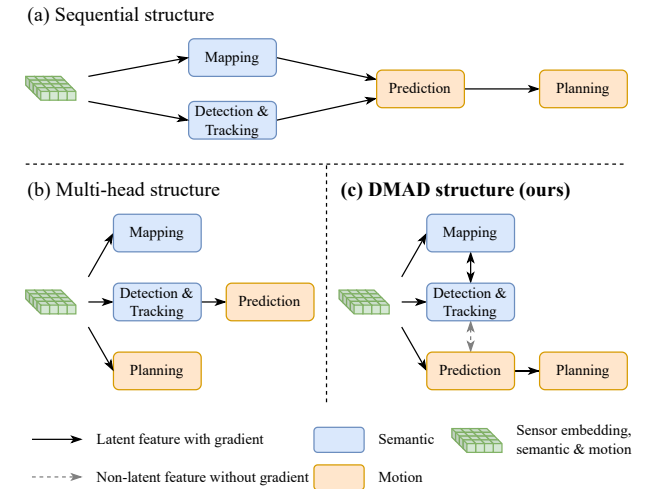


Figure 1. **Comparison of E2E structures.** In (a), semantic and motion learning occur sequentially. In (b), the multi-head structure parallelizes tasks with different heads; however, motion and semantic learning remain sequential in detection, tracking, and prediction. In (c), semantic and motion learning are performed in parallel without latent feature sharing or gradient propagation. In contrast, the exchange of information between the object and map perception modules is enhanced.

these approaches exhibit negative transfer of object detection and tracking. In other words, the perception performance of jointly trained E2E models is typically inferior to that of models trained without the motion prediction and planning tasks.

We analyze the underlying causes of negative transfer by inspecting the types of learned heterogeneous information: semantic and motion. Semantic information encompasses the categories of surrounding objects, lanes, crossings and *etc.*, while motion information describes the temporal changes occurring within the environment. Sequential methods [15, 21, 22, 55] execute the two processes in succession, first conducting detection and tracking, and then utilizing the features representing an object for trajectory prediction. This sequential design forces the features to

encompass motion information, compromising the initially learned semantic information. It consequently leads to a negative transfer of perception. Another structure executes most tasks with different heads in parallel, as depicted in Fig. 1b, *e.g.*, PARA-Drive [48] and NMP [51]. However, since detection and prediction remain sequential, the issue of negative transfer persists.

In this work, we propose **DMAD structure** (Fig. 1c), **D**ividing and **M**erging motion and semantic learning for E2E Autonomous **D**riving. DMAD addresses the issue of negative transfer by separating semantic and motion learning. Furthermore, it leverages correlations among semantic tasks by merging them.

For dividing, we propose **Neural-Bayes motion decoder**. We maintain a set of motion queries that attend to the bird’s-eye view (BEV) features parallel to the object (detection & tracking) queries. The key difference between motion queries and object queries is that they are decoded into past and future trajectories rather than bounding boxes with classes. Motion and object queries share a single set of reference points, updated recursively by detection and prediction. It allows only limited information exchange between both types of queries, mediated through the reference points without gradient flow. Moreover, we calculate the object’s velocity using the predicted trajectory with finite differences, thereby removing the requirement for object queries to learn the velocity directly. In this manner, the object query focuses on learning semantic and appearance features, while the motion query is dedicated to capturing motion features. The two types of heterogeneous information are learned separately along distinct paths, effectively preventing negative transfer. Notably, the DMAD structure promotes motion learning to the same level of semantic learning, treating detection, tracking, and prediction as concurrent tasks for the first time, to the best of our knowledge.

For merging, we propose **interactive semantic decoder** to enhance the exchange of semantic insights in detection and map segmentation. Object perception and map perception are inherently related tasks. Previous methods have often overlooked this connection, typically executing the two along parallel paths [21, 22, 55]. DualAD [15] leverages this correlation but allows only object perception to learn from the map. Our method uses layer-wise iterative self-attention [43] to enable mutual learning between object and map tasks, fostering positive transfer.

Building on UniAD [21], experiments on the nuScenes dataset showcase the effectiveness of DMAD structure in mitigating negative transfer. Our approach achieves significant performance gains in perception and prediction. Without modifying the planning module, we demonstrate how improved perception and prediction benefit planning in open-loop evaluation, achieving state-of-the-art (SOTA) collision metrics.

Our key contributions are summarized as follows:

- We propose DMAD, a modular E2E AD paradigm that divides and merges tasks according to the information they are supposed to learn. This design eliminates negative transfer between different types of tasks while reinforcing positive transfer among similar tasks.
- We introduce the Neural-Bayes motion decoder to perform trajectory prediction concurrently with object detection and tracking, and the interactive semantic decoder to enhance information sharing between object and map perception.
- We validate the effectiveness of our approach, which builds on UniAD [21], on the nuScenes [3] dataset. It yields improved perception and prediction results and SOTA collision rates in open-loop planning.

## 2. Related Work

**Semantic learning.** Semantic learning includes object detection and map segmentation. Multi-view cameras have become popular due to their cost-effectiveness and strong capability in capturing semantic information. Current SOTA object detection and mapping approaches are built on the DETR [4] architecture, utilizing a set of queries to extract semantic information from environment features through cross-attention [43] mechanisms. Sparse methods [29, 46] learn semantic information by projecting queries onto the corresponding image features, focusing on the relevant regions. The PETR series [31, 32, 45] embeds 3D positional encoding directly into 2D image features, eliminating the need for query projection. Another line of work aggregates all image features into a BEV feature [23, 27, 28, 38, 39, 49]. Propagating the object queries over time enables multi-object tracking [35, 50]. This concept is also utilized in map perception [9]. It is important to note that tracking is also a motion-related task. However, in query-based trackers, velocities are the only motion information to be learned. Therefore, we classify it as a semantic task. We adopt the encoder from BEVFormer [23] and the query propagation mechanism from MOTR [50] while employing entirely novel decoders.

**Motion learning.** By motion, we refer to trajectory prediction and planning. Trajectory prediction studies typically use the ground truth of objects’ historical trajectories along with high-definition maps as inputs. Early approaches [1, 7, 13] rasterize maps and trajectories into a BEV image, using CNNs to extract scene features. Vectorized methods [17, 56] represent elements using polygons and polylines, using GNNs or Transformers to encode the scene [18, 36, 41, 44, 53].

For planning, imitation learning is a straightforward approach to E2E planning, where a neural network is trained to plan future trajectories or control signals directly

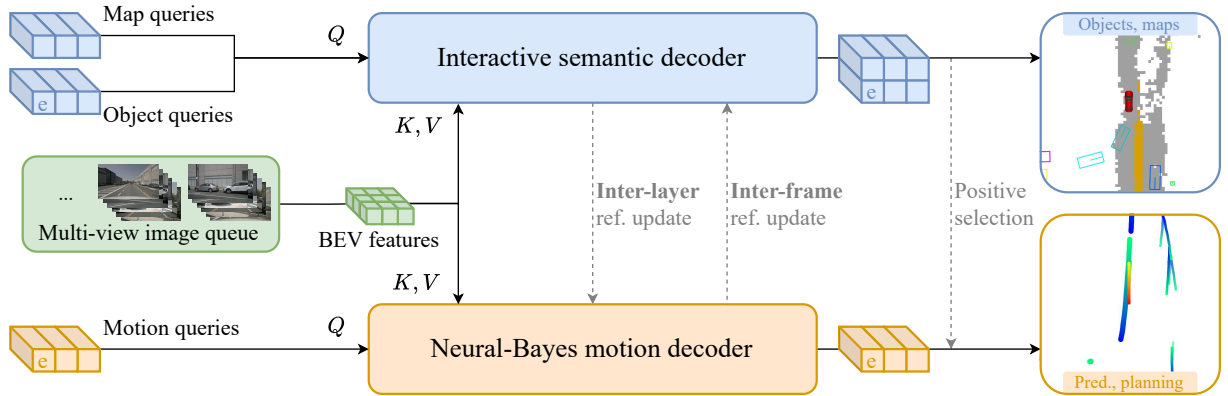


Figure 2. **An overview of DMAD.** Given multi-view images as input, a BEV encoder extracts the BEV features. Map and object queries are initialized, then interactively attend to the BEV features for map and object perception. Motion queries are mapped one-to-one with object queries, sharing reference points. These reference points are iteratively updated. Finally, the motion queries are selected based on the existence of their corresponding objects and decoded into future trajectories. The motion query with “e”, representing the ego vehicle, is used for planning. The gray dashed line arrows indicate operations without gradient flow.

from sensor data, minimizing the distance between the planned path and the expert driving policy [2, 8, 40]. Many approaches incorporate semantic tasks as auxiliary components to support E2E planning, using the nuScenes [3] dataset and open-loop evaluation. These methods extend beyond pure motion learning and will be explored in the next paragraph. AD-MLP [52] and Ego-MLP [25] utilize only the ego vehicle’s past motion states and surpass methods that rely on sensor inputs in open-loop evaluation. It aligns with our argument that semantics and motion are heterogeneous: AD-MLP and Ego-MLP can concentrate on learning from expert motion data without interference by irrelevant semantic information, thereby achieving superior open-loop planning performance.

**Joint semantic and motion learning.** E2E perception and prediction approaches are typically learning semantics and motion jointly. The pioneering work FaF [34] uses a prediction head, in addition to the detection head, to decode the object features into future trajectories. Some works [5, 14, 16] enhance it with intention-based prediction and refinement. PnPNet [26] and PTP [47] involve tracking, *i.e.*, jointly optimizing detection, association, and prediction tasks. While PTP performs tracking and prediction in parallel, it cannot predict newly emerging objects due to the lack of concurrent detection—a limitation our method successfully overcomes. ViP3D [19] first extends the query-based detection and tracking framework [50] to prediction. Each query represents an object and propagates across frames. In each frame, queries are decoded into bounding boxes and trajectories with the assistance of high-definition maps.

To include planning, NMP [51] extends IntentNet [5] with a sampling-based planning module, where prediction

is leveraged to minimize collisions during the planning process. Other works, such as [6, 10, 20], incorporate map perception as an auxiliary task. With the growing popularity of query-based object detectors [4, 23] and trackers [35, 50], recent modular E2E AD approaches represent objects as queries, similar to ViP3D [19]. UniAD [21] and its variants [15, 48] retain the query propagation mechanism for tracking, aiming to explicitly model objects’ historical motion. In contrast, VAD [22] and GenAD [55] do not perform tracking, predicting trajectories based on the temporal information embedded within the BEV feature. The main issue with these methods is that they attempt to use a single feature (query) to represent an object’s appearance and motion. Compared to pure semantic learning, motion occupies a portion of the feature channels but fails to contribute to perception, resulting a negative transfer of the perception module. Our work effectively addresses this issue.

### 3. Method

Figure 2 shows an overview of DMAD structure, which builds upon UniAD [21]. A BEV feature is extracted from multi-view camera images [23] and is the shared feature across all tasks, including detection, tracking, mapping, prediction, and planning. We initialize three distinct types of queries—object, map, and motion—which attend to the BEV feature to extract the specific information required for each respective task. Based on the type of information learned, the decoding process is divided into two pathways. On one way, object and map decoding are jointly performed within the **Interactive semantic decoder**, where both types of queries iteratively exchange latent semantic information at each decoding layer, as introduced in Sec. 3.1. On the

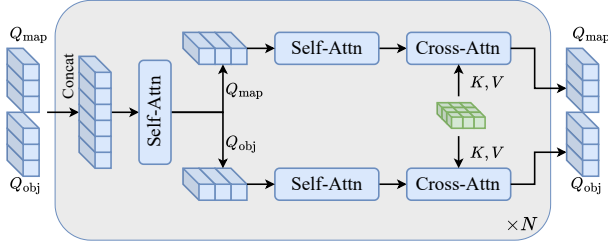


Figure 3. **Interactive semantic decoding.** Object and map queries are concatenated and interact through a self-attention module before being separated to independently attend to the BEV features. This process is repeated across  $N$  stacked layers.

other way, motion queries extract motion information from the BEV feature within the **Neural-Bayes motion decoder**. Each motion query corresponds directly to an object query. The motion query uses the object’s coordinates as the reference point at each decoding layer. After decoding each frame, the predicted future waypoint from the motion query serves as the reference point for the object query in the subsequent frame. This recursive structure is similar to the behavior of Bayes filter [42]. The exchange of reference points is always without gradient, as elaborated in Sec. 3.2. At last, motion queries are passed on to the planning module. The system is fully E2E trainable, with motion and semantic gradients propagated in distinct paths.

### 3.1. Interactive Semantic Decoder

Previous studies [21, 55] essentially treat object detection and map perception as separate tasks. However, there are correlations between objects and map elements. For instance, the position of a vehicle is highly likely to be within a drivable area, and the orientation of cars on a lane is likely to align with the direction of the lane. To leverage this semantic correlation, we introduce the Interactive Semantic Decoder. In contrast to the unidirectional interaction in DualAD [15], our approach enables a bidirectional exchange of information.

We initialize a set of object queries  $Q_{obj} \in \mathbb{R}^{N_{obj} \times d}$  and a set of map queries  $Q_{map} \in \mathbb{R}^{N_{map} \times d}$ . The number of queries could be different, while the dimensions  $d$  must be the same. Each decoding layer first concatenates both types of queries. Self-attention [43] is then applied, where both tasks exchange their semantic information. Subsequently, the two types of queries are divided, each performing self-attention and cross-attention on the BEV features, respectively, as shown in Fig. 3.

After interactive semantic decoding, we decode map queries into dense representations, in line with Panoptic Segformer [24]. Each object query is classified into a category  $c$  and regressed into a vector  $[\Delta x, \Delta y, \Delta z, w, h, l, \theta]^T$ . Each object query is associated

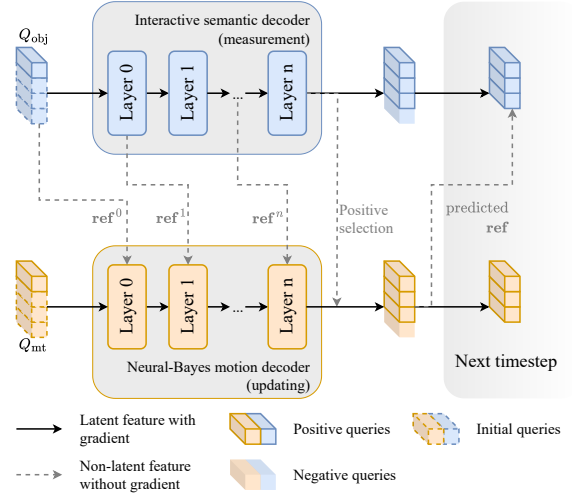


Figure 4. **Neural-Bayes motion decoding.** After each decoding layer, the semantic decoder updates the reference points, which are then shared with the motion decoder. At the end of each frame, positive object query indices are used to select corresponding motion queries. These positive object and motion queries are propagated to the subsequent frame, with the motion query predictions serving as reference points for the next frame. Map queries, ego queries and BEV features are omitted for simplicity.

with a reference point  $[x_{ref}, y_{ref}, z_{ref}]^T$ . Rather than directly learning the absolute coordinates of the object, it learns the offsets relative to its corresponding reference points. Thus, the bounding boxes can be represented as  $[x_{ref} + \Delta x, y_{ref} + \Delta y, z_{ref} + \Delta z, w, h, l, \theta]^T$ . Notably, velocities are not regressed, as they pertain to motion information. We design the object queries to focus solely on semantic information, *i.e.*, the object’s category, center point, size, and orientation.

### 3.2. Neural-Bayes Motion Decoder

The motion refers to the change of semantics over time. Safe and comfortable driving necessitates that the AD system comprehends environmental changes and anticipates future developments, making decisions accordingly. For current modular E2E systems, the motion task refers to trajectory prediction and motion planning. We introduce a novel motion decoder operating in parallel with the semantic decoder, aimed at fully decoupling motion and semantic learning to reduce the negative transfer of semantic tasks. Given the correlation between motion and semantics, we design a recursive process to facilitate the exchange of human-readable information between the two decoders analogous to the Bayes filter [42].

**Bayes filter.** We begin with a brief introduction to the Bayes filter as a preliminary. Bayes filter estimates an un-

known distribution based on the process model and noisy measurements. It can be formulated as follows:

$$p(\mathbf{x}_t | \mathbf{z}_{1:t}) = p(\mathbf{z}_t | \mathbf{x}_t) p(\mathbf{x}_t | \mathbf{z}_{1:t-1}), \quad (1)$$

where  $\mathbf{x}$  denotes the state,  $\mathbf{z}$  represents the measurement, and the subscript indicates timesteps. The task of Bayes filter is to estimate the state  $\mathbf{x}_t$  at timestep  $t$  given all the measurements  $\mathbf{z}_{1:t}$  in the past from timestep 1 to  $t$ , which is the product of the likelihood  $p(\mathbf{z}_t | \mathbf{x}_t)$  and the prediction  $p(\mathbf{x}_t | \mathbf{z}_{1:t-1})$ .

In the context of multiple object tracking, this process can be carried out in three steps: first, predicting the current position based on the object’s historical states  $\mathbf{x}_{1:t-1}$ ; second, identifying the detection most likely to match the prediction as the measurement; and finally, updating the current state  $\mathbf{x}_t$  according to the latest measurement  $\mathbf{z}_{t-1}$ . This process is recursively executed over successive timesteps.

Next, we present the proposed Neural-Bayes motion decoder. As illustrated in Fig. 4, our method also comprises the processes of prediction, measurement, and updating.

**Initialization.** The Neural-Bayes Motion Decoder is a Transformer decoder. We initialize a set of motion queries  $Q_{\text{mt}} \in \mathbb{R}^{N_{\text{mt}} \times d}$  in the same way we initialize object queries. The motion queries correspond one-to-one with the object queries, *i.e.*,  $N_{\text{mt}} = N_{\text{obj}}$ . However, since they do not directly interact in the latent space, their dimensionalities  $d$  can differ. Each motion query represents the motion state of an object, although the model does not initially know whether the object exists. Additionally, motion queries and object queries share a common set of reference points.

**Measurement.** The detection, already introduced in Sec. 3.1, is treated as the measurement in Bayes filter. After each semantic decoding layer, the object queries are regressed, yielding the coordinate vectors  $\mathbf{ref} = [x, y, z]^T$  of the tentative object, which then serves as reference points for the next layer:

$$\mathbf{ref}^{l+1} = \text{Regression}(\text{Semantic-Dec}^l(Q_{\text{obj}}^l, BEV, \mathbf{ref}^l)), \quad (2)$$

where the superscript denotes the layer.

**Updating.** With the reference points  $\mathbf{ref}^l$  from the semantic decoding (the inter-layer reference points update in Fig. 2), the motion queries also attend to the BEV feature via cross-attention:

$$Q_{\text{mt}}^{l+1} = \text{Motion-Dec}^l(Q_{\text{mt}}^l, BEV, \mathbf{ref}^l), \quad (3)$$

where the motion queries are updated conditioned on the measured reference points.

**Prediction.** We employ multilayer perceptrons (MLPs) to extract trajectories from the motion queries. It is worth noting that motion extraction occurs in two stages: first through the unimodal trajectory construction, followed by the multimodal prediction.

The first stage aims to compute the unimodal velocity and future reference points, guiding the motion query to learn aggregated motion states from the past and enabling the prediction of the near future. It produces a single trajectory spanning from the past timestep  $t_{\text{past}}$  to the future timestep  $t_{\text{fut-1}}$ . The velocity is calculated using the finite difference method based on the waypoints surrounding the current timestep. We use the first future waypoint as the initial reference point for the object query in the next frame, *i.e.*, inter-frame reference points update in Fig. 2, for object tracking.

In the second stage, we follow UniAD for multimodal intention modeling, generating multiple future trajectories within the future  $t_{\text{fut-2}}$  timesteps, along with their corresponding confidence scores.

**Tracking.** Multi-object tracking is conducted concurrently with detection, as proposed in MOTR [50]. During training, object queries associated with ground truth are referred to as positive queries; during inference, positivity is determined by whether the confidence score exceeds a specified threshold. Positive object queries are selected and propagated over time into future timesteps, concatenated with initial queries. The same applies to motion queries because they are in relation. This mechanism enables continuous predicting, measuring, and updating, similar to the Bayes filter.

## 4. Experiments

We conduct experiments on the nuScenes [3] dataset to validate the effectiveness of our method. We present results in three parts. The first focuses on perception (detection, tracking, and mapping). We compare perception performance across two training stages to demonstrate that our method mitigates the negative transfer. In the second part, we evaluate motion prediction and planning. We verify the benefits of our method for open-loop planning without modifying the planning module. Lastly, we provide an extensive ablation study.

### 4.1. Training Configuration

This subsection outlines the differences between our experimental setup and the default UniAD training configuration and the rationale behind these adjustments.

**Two-stage training.** We follow the two-stage training scheme of UniAD. In the first stage, we train object detection, tracking, and mapping. In the second stage,

Method	NDS $\uparrow$	mAP $\uparrow$	mAVE $\downarrow$
VAD [22]	0.460	0.330	<u>0.405</u>
GenAD [55]	0.280	0.213	0.669
PARA-Drive [48]	0.480	0.370	-
UniAD - stage 1	0.497	0.382	0.411
UniAD - stage 2	0.491 (-1.2%)	0.377 (-1.3%)	0.412 (+0.2%)
DMAD - stage 1	<u>0.504</u>	<u>0.395</u>	0.406
DMAD - stage 2	<b>0.506 (+0.4%)</b>	<b>0.396 (+0.3%)</b>	<b>0.395 (-2.7%)</b>

Table 1. **Object detection results.** The results of VAD are from the official repository. The performance changes in stage 2 are expressed as percentages, with **red** indicating a decline and **blue** representing improvement.

Method	AMOTA $\uparrow$	AMOTP $\downarrow$	IDS $\downarrow$
ViP3D [19]	0.217	1.63	-
MUTR3D [54]	0.294	1.50	3822
PARA-Drive [48]	0.350	-	-
UniAD - stage 1	0.374	<u>1.31</u>	816
UniAD - stage 2	0.354 (-5.3%)	1.34 (+2.3%)	1381 (+69%)
DMAD - stage 1	<b>0.394</b>	1.32	<u>781</u>
DMAD - stage 2	<u>0.393 (-0.3%)</u>	<b>1.30 (-1.5%)</b>	<b>767 (-1.8%)</b>

Table 2. **Multi-object tracking results.**

all modules are trained, with the BEV feature extraction frozen. Notably, in our approach, since tracking relies on reference points provided by unimodal prediction, the training of unimodal prediction is included in the first stage. Multimodal prediction is trained only in the second stage, which is consistent with UniAD.

**Queue length.** Since AD is a time-dependent task, the model typically uses a sequence of consecutive frames as a training sample. The number of input frames, *i.e.*, queue length  $q$ , directly determines the temporal horizon the model can capture, affecting related tasks’ performance. However, UniAD employs different queue lengths across its two training stages: 5 in the first stage and 3 in the second. The reduced queue length in the second stage also reduces perception performance because of less temporal aggregation. It interferes with identifying the negative transfer effects inherent to the model. To mitigate this interference, we standardize the queue length to 3 across both training stages. Unless otherwise specified, the performance of UniAD in all result tables is reproduced with a queue length of 3 using the official codebase [11].

## 4.2. Perception

**Metrics.** For object detection and tracking, we use the metrics defined in the nuScenes benchmark. The primary metrics for detection are nuScenes Detection Score (NDS) and mean average precision (mAP). NDS provides a holistic

Method	Lanes $\uparrow$	Drivable $\uparrow$	Dividers $\uparrow$
VPN [37]	0.180	<u>0.760</u>	-
LSS [39]	0.183	<u>0.739</u>	-
BEVFormer [23]	0.239	<b>0.775</b>	-
PARA-Drive [48]	<b>0.330</b>	0.710	-
UniAD - stage 1	0.293	0.650	0.248
UniAD - stage 2	0.312 (+6.5%)	0.678 (+4.3%)	<u>0.267 (+7.7%)</u>
DMAD - stage 1	0.292	0.655	0.242
DMAD - stage 2	<u>0.321 (+9.9%)</u>	0.691 (+5.5%)	<b>0.271 (+12%)</b>

Table 3. **Map segmentation results.**

Method	EPA $\uparrow$		minADE $\downarrow$	
	C	P	C	P
PnPNet [26]	0.222	-	1.15	-
ViP3D [19]	0.226	-	2.05	-
GenAD [55]	<b>0.588</b>	0.352	0.84	0.84
UniAD	0.495	<u>0.361</u>	<b>0.69</b>	<u>0.79</u>
DMAD	<u>0.535 (+8.1%)</u>	<b>0.416 (+15%)</b>	<u>0.72 (+4.3%)</u>	<b>0.77 (-2.5%)</b>

Table 4. **Trajectory prediction results.** C and P stand for cars and pedestrians respectively. We indicate improvements to UniAD with **blue**, and declines with **red**.

evaluation of detection performance by considering both detection precision and true positive errors of bounding boxes, such as translation, orientation, and velocity errors. For multiple object tracking, we report the average multi-object tracking accuracy (AMOTA) and the average multi-object tracking precision (AMOTP). The former provides a comprehensive evaluation of tracking performance by considering ID switches, false positives, and false negatives, while the latter measures the localization error of the tracked objects.

For mapping, we use the intersection over union (IoU) metric to evaluate the segmentation of drivable areas, lanes, and dividers.

**Object detection.** Table 1 presents the detection performance across two training stages. After the second stage of training, UniAD’s performance shows a slight decline, with NDS decreasing by 1.2% and mAP by 1.3%. In contrast, our method demonstrates improvements of 0.4% and 0.3%, respectively. In the first stage, thanks to the interactive semantic decoding, our approach outperforms UniAD by 1.4% in NDS and 3.4% in mAP. In the second stage, with the benefit of separated motion learning mitigating negative transfer, our method finally surpasses UniAD by 3.1% in NDS and 5.0% in mAP.

**Multi-object tracking.** Appearance and motion are two important cues for multi-object tracking. Due to using a single feature vector to represent appearance and motion, UniAD exhibits a negative transfer of 5.3% in AMOTA

Method	Perception tasks	Ego states in planner	L2 distances (m) ↓				Collision rates (%) ↓			
			1s	2s	3s	Avg.	1s	2s	3s	Avg.
Ego-MLP [52]	✗	✓	0.17	0.34	0.60	0.370	0 <sup>†</sup>	0.27 <sup>†</sup>	0.85 <sup>†</sup>	0.373 <sup>†</sup>
AD-MLP [25]	✗	✓	0.14	0.10	0.41	0.217	0.10	0.10	0.17	0.123
VAD [22]	✓	✗	0.41	0.70	1.05	0.720	<b>0.07</b>	0.17	0.41	0.217
DualVAD [15]	✓	✗	0.30	0.53	0.82	0.550	0.11	0.19	0.36	0.220
GenAD [55]	✓	✗	<u>0.28</u>	<u>0.49</u>	<u>0.78</u>	<u>0.517</u>	<u>0.08</u>	0.14	0.34	0.187
UniAD* [21]	✓	✗	0.42	0.63	0.91	0.656	<b>0.07</b>	<b>0.10</b>	<u>0.22</u>	<u>0.130</u>
PARA-Drive [48]	✓	✗	<b>0.25</b>	<b>0.46</b>	<b>0.74</b>	<b>0.483</b>	0.14	0.23	0.39	0.253
UniAD	✓	✗	0.48	0.76	1.12	0.784	<b>0.07</b>	<u>0.11</u>	0.27	0.150
DMAD	✓	✗	0.38	0.60	0.89	0.625 (-20%)	<b>0.07</b>	0.12	<b>0.19</b>	<b>0.127 (-15%)</b>

Table 5. **Open-loop planning.** Ego-MLP and AD-MLP are faded since both learn only the ego motion. \*Results from the checkpoint in the official repository [11], trained with a queue length of 5 in stage 1. †Ego-MLP employs a different strategy in the evaluation of collision rates, therefore the results are not comparable.

and 2.3% in AMOTP, as shown in Tab. 2. Our dividing design enables object queries to learn about appearance more effectively. At the same time, unimodal predictions offer enhanced tracking reference points compared to the velocity-based reference point updating in UniAD. Consequently, our method surpasses UniAD in the first stage and remains unaffected by negative transfer in the second stage, achieving a gain of 11.0% in AMOTA and 3.0% in AMOTP.

**Map segmentation.** Mapping is the only perception task that does not exhibit negative transfer in UniAD. Leveraging the advantages of interactive semantic decoding, our method marginally surpasses UniAD in IoU performance across drivable areas, lanes, dividers, and crossings (see Tab. 3).

### 4.3. Prediction and Planning

**Metrics.** For motion prediction, we utilize E2E perception accuracy (EPA) proposed in ViP3D [19] as the main metric. We also report the traditional minimum average displacement error (minADE). However, since minADE is a true positive metric, it does not fully capture the predictive capabilities of the E2E system, whereas EPA accounts for the number of false positives. For open-loop planning, we utilize L2 distances and collision rates in 1, 2, and 3 seconds.

**Trajectory prediction.** We report car and pedestrian prediction metrics in Tab. 4. Our method demonstrates a significant improvement in EPA, with enhancements of 8.1% for cars and 15% for pedestrians. This improvement is attributed to our design, which eliminates the negative transfer of object detection and tracking, thereby reducing many false negatives. In terms of minADE, our method only slightly outperforms UniAD for pedestrians. A potential reason might be that, after reaching a certain threshold

in detection performance, further detection improvements often reduce false positives by successfully detecting challenging objects that are either distant or occluded. For such difficult objects, coordinate errors may be larger, and the historical motion information of the objects could be very limited and inaccurate. These inaccuracies significantly increase the difficulty of prediction. A similar situation is observed in UniAD [21]: in the supplementary materials, UniAD-Large substantially surpasses UniAD-Base in EPA (thanks to better detection and tracking performance), yet it falls short of UniAD-Base in minADE.

**Open-loop planning.** We adopt the evaluation method of VAD [22]. Despite certain criticisms [25, 48, 52], it accommodates the widest range of methods to our knowledge. We report a comprehensive comparison in Tab. 5. Notably, jointly optimizing L2 distances and collision rates proves challenging. While PARA-Drive achieves the lowest L2 distances, it also exhibits the highest collision rates. Our method significantly outperforms UniAD, reducing L2 distances by 20% and collision rates by 15%. Furthermore, it surpasses the original UniAD configuration with a longer queue length, achieving SOTA collision rate performance.

### 4.4. Ablation Study

We conduct an extensive ablation study on the proposed decoders, as shown in Tab. 6. We decompose the motion decoder into three components: motion query, inter-layer, and inter-frame reference point updating.

**Model profile.** In methods with multi-view camera images as inputs, the primary computational cost is concentrated in the image backbone [23]. In contrast, our approach focuses on the decoding component, resulting in minimal impact on model size and speed. Compared to UniAD [21], our decoders increase 5.4M parameters and 0.02 seconds

Method ID	Interactive semantic dec.	Motion queries	Inter-layer ref. update	Inter-frame ref. update	#Params (M)	Inference time (s)	NDS $\uparrow$	AMOTA $\uparrow$	Lanes $\uparrow$	EPA $\uparrow$	Avg. L2 $\downarrow$	Avg. Col. $\downarrow$
1 (UniAD)	$\times$	$\times$	$\times$	$\times$	135.0	0.47	0.491	0.354	0.312	0.495	0.784	0.150
2	$\checkmark$	$\times$	$\times$	$\times$	135.1	0.48	0.503	0.382	0.320	0.524	0.683	0.150
3	$\times$	$\checkmark$	$\checkmark$	$\checkmark$	140.3	0.49	0.502	0.387	0.313	<b>0.535</b>	0.661	0.143
4	$\checkmark$	$\checkmark$	$\times$	$\times$	140.4	0.49	0.481	0.339	0.322	0.485	0.655	0.163
5	$\checkmark$	$\checkmark$	$\checkmark$	$\times$	140.4	0.49	0.489	0.352	<b>0.323</b>	0.498	0.648	0.160
6	$\checkmark$	$\checkmark$	$\times$	$\checkmark$	140.4	0.49	0.495	0.364	0.319	0.512	0.631	0.137
7 (DMAD)	$\checkmark$	$\checkmark$	$\checkmark$	$\checkmark$	140.4	0.49	<b>0.506</b>	<b>0.393</b>	0.321	<b>0.535</b>	<b>0.625</b>	<b>0.127</b>

Table 6. Ablation of DMAD.



Figure 5. **Visualizations.** DMAD utilizes multi-view camera inputs to conduct object detection & tracking, map segmentation, trajectory prediction, and planning. In the map visualization, gray, yellow, and purple indicate drivable areas, lane dividers, and pedestrian crossings. The red-yellow trajectory represents planning outputs within 3 seconds, while the blue-green trajectories illustrate predictions within 6 seconds. We display three potential predictions, with fading intensity indicating decreasing probability.

of inference latency on an NVIDIA RTX 6000 Ada.

**Effect of dividing and merging.** Experiments ID 1, 2, 3, 7 demonstrate the effectiveness of both proposed decoders. The standalone application of the interactive semantic decoder (ID 2) significantly enhances the performance of object detection, tracking, and map segmentation. The standalone application of the Neural-Bayes motion decoder (ID 3) markedly improves prediction and planning. Notably, ID 3 also significantly enhances detection and tracking, attributed to freeing object queries from learning velocities and the higher-quality reference points provided by the unimodal prediction. Experiments ID 4, 5, 6, 7 show the importance of inter-layer and inter-frame updating in the Neural-Bayes motion decoder. An incomplete Neural-Bayes motion decoder (ID 4, 5, 6) undermines detection and tracking results. Only combining both updates enables the model to achieve optimal performance.

#### 4.5. Visualizations

Figure 5 shows the results of DMAD at a complex intersection. DMAD accurately detects and tracks densely packed vehicles and pedestrians and predicts the future behavior of each object considering the perceived map information.

## 5. Conclusion

We introduce DMAD, a novel modular E2E AD architecture that divides semantic and motion learning while integrating semantic tasks. By decoupling the semantic and motion learning of objects, DMAD eliminates the negative transfer that E2E training typically imposes on object detection and tracking. Besides, we leverage the correlation between semantic tasks to promote positive transfer during E2E training. Without modifying the planning module, our improvements in perception and prediction directly enhance planning performance, resulting in lower L2 distances and SOTA collision rates. In the future, it is worthwhile to evaluate our approach with closed-loop planning.

**Acknowledgments:** The authors thank Stellantis, Opel Automobile GmbH for the fruitful collaboration and the opportunity to contribute to the “STADT:up” project (FKZ 19A22006P) funded partly by the German Federal Ministry for Economic Affairs and Climate Action (BMWK) and the European Union. The authors also thank the project “NXT GEN AI METHODS” funded by the BMWK and gratefully acknowledge the computing resources supported by the Helmholtz Association’s Initiative and Networking Fund on HAICORE@FZJ and by the Federal Ministry of Education and Research and the Ministry of Science, Research and Arts Baden-Württemberg on HoreKa at NHR@KIT.



## References

- [1] Mayank Bansal, Alex Krizhevsky, and Abhijit Ogale. ChauffeurNet: Learning to Drive by Imitating the Best and Synthesizing the Worst. In *Robotics: Science and Systems*, 2019. 2
- [2] Mariusz Bojarski. End to End Learning for Self-Driving Cars. *arXiv preprint arXiv:1604.07316*, 2016. 3
- [3] Holger Caesar, Varun Bankiti, Alex H Lang, Sourabh Vora, Venice Erin Liong, Qiang Xu, Anush Krishnan, Yu Pan, Giancarlo Baldan, and Oscar Beijbom. nuScenes: A multimodal dataset for autonomous driving. In *CVPR*, pages 11621–11631, 2020. 2, 3, 5, 1
- [4] Nicolas Carion, Francisco Massa, Gabriel Synnaeve, Nicolas Usunier, Alexander Kirillov, and Sergey Zagoruyko. End-to-End Object Detection with Transformers. In *ECCV*, pages 213–229, 2020. 2, 3
- [5] Sergio Casas, Wenjie Luo, and Raquel Urtasun. IntentNet: Learning to Predict Intention from Raw Sensor Data. In *CoRL*, pages 947–956, 2018. 3
- [6] Sergio Casas, Abbas Sadat, and Raquel Urtasun. MP3: A Unified Model to Map, Perceive, Predict and Plan. In *CVPR*, pages 14403–14412, 2021. 3
- [7] Yuning Chai, Benjamin Sapp, Mayank Bansal, and Dragomir Anguelov. MultiPath: Multiple Probabilistic Anchor Trajectory Hypotheses for Behavior Prediction. In *CoRL*, 2019. 2
- [8] Dian Chen and Philipp Krähenbühl. Learning from All Vehicles. In *CVPR*, pages 17222–17231, 2022. 3
- [9] Jiacheng Chen, Yuefan Wu, Jiaqi Tan, Hang Ma, and Yasutaka Furukawa. MapTracker: Tracking with Strided Memory Fusion for Consistent Vector HD Mapping. In *ECCV*, pages 90–107, 2025. 2
- [10] Kashyap Chitta, Aditya Prakash, and Andreas Geiger. NEAT: Neural Attention Fields for End-to-End Autonomous Driving. In *ICCV*, pages 15793–15803, 2021. 3
- [11] UniAD contributors. Planning-oriented Autonomous Driving. <https://github.com/OpenDriveLab/UniAD>, 2023. 6, 7
- [12] Michael Crawshaw. Multi-Task Learning with Deep Neural Networks: A Survey. *arXiv preprint arXiv:2009.09796*, 2020. 1
- [13] Henggang Cui, Vladan Radosavljevic, Fang-Chieh Chou, Tsung-Han Lin, Thi Nguyen, Tzu-Kuo Huang, Jeff Schneider, and Nemanja Djuric. Multimodal Trajectory Predictions for Autonomous Driving using Deep Convolutional Networks. In *ICRA*, pages 2090–2096, 2019. 2
- [14] Nemanja Djuric, Henggang Cui, Zhaoen Su, Shangxuan Wu, Huahua Wang, Fang-Chieh Chou, Luisa San Martin, Song Feng, Rui Hu, Yang Xu, et al. MultiXNet: Multiclass Multistage Multimodal Motion Prediction. In *IEEE Intelligent Vehicles Symposium (IV)*, pages 435–442, 2021. 3
- [15] Simon Doll, Niklas Hanselmann, Lukas Schneider, Richard Schulz, Marius Cordts, Markus Enzweiler, and Hendrik Lensch. DualAD: Disentangling the Dynamic and Static World for End-to-End Driving. In *CVPR*, pages 14728–14737, 2024. 1, 2, 3, 4, 7
- [16] Sudeep Fadadu, Shreyash Pandey, Darshan Hegde, Yi Shi, Fang-Chieh Chou, Nemanja Djuric, and Carlos Vallespi-Gonzalez. Multi-View Fusion of Sensor Data for Improved Perception and Prediction in Autonomous Driving. In *Proceedings of the IEEE/CVF Winter Conference on Applications of Computer Vision*, pages 2349–2357, 2022. 3
- [17] Jiyang Gao, Chen Sun, Hang Zhao, Yi Shen, Dragomir Anguelov, Congcong Li, and Cordelia Schmid. VectorNet: Encoding HD Maps and Agent Dynamics From Vectorized Representation. In *CVPR*, pages 11525–11533, 2020. 2
- [18] Junru Gu, Chen Sun, and Hang Zhao. DenseTNT: End-to-end Trajectory Prediction from Dense Goal Sets. In *ICCV*, pages 15303–15312, 2021. 2
- [19] Junru Gu, Chenxu Hu, Tianyuan Zhang, Xuanyao Chen, Yilun Wang, Yue Wang, and Hang Zhao. ViP3D: End-to-end Visual Trajectory Prediction via 3D Agent Queries. In *CVPR*, pages 5496–5506, 2023. 3, 6, 7, 1
- [20] Shengchao Hu, Li Chen, Penghao Wu, Hongyang Li, Junchi Yan, and Dacheng Tao. ST-P3: End-to-end Vision-based Autonomous Driving via Spatial-Temporal Feature Learning. In *ECCV*, pages 533–549, 2022. 3
- [21] Yihan Hu, Jiazhi Yang, Li Chen, Keyu Li, Chonghao Sima, Xizhou Zhu, Siqi Chai, Senyao Du, Tianwei Lin, Wenhai Wang, et al. Planning-oriented Autonomous Driving. In *CVPR*, pages 17853–17862, 2023. 1, 2, 3, 4, 7
- [22] Bo Jiang, Shaoyu Chen, Qing Xu, Bencheng Liao, Jiajie Chen, Helong Zhou, Qian Zhang, Wenyu Liu, Chang Huang, and Xinggang Wang. VAD: Vectorized Scene Representation for Efficient Autonomous Driving. In *ICCV*, pages 8340–8350, 2023. 1, 2, 3, 6, 7
- [23] Zhiqi Li, Wenhai Wang, Hongyang Li, Enze Xie, Chonghao Sima, Tong Lu, Yu Qiao, and Jifeng Dai. BEVFormer: Learning Bird’s-Eye-View Representation from Multi-Camera Images via Spatiotemporal Transformers. In *ECCV*, pages 1–18, 2022. 2, 3, 6, 7
- [24] Zhiqi Li, Wenhai Wang, Enze Xie, Zhiding Yu, Anima Anandkumar, Jose M Alvarez, Ping Luo, and Tong Lu. Panoptic SegFormer: Delving Deeper into Panoptic Segmentation with Transformers. In *CVPR*, pages 1280–1289, 2022. 4
- [25] Zhiqi Li, Zhiding Yu, Shiyi Lan, Jiahao Li, Jan Kautz, Tong Lu, and Jose M Alvarez. Is Ego Status All You Need for Open-Loop End-to-End Autonomous Driving? In *CVPR*, pages 14864–14873, 2024. 3, 7
- [26] Ming Liang, Bin Yang, Wenyuan Zeng, Yun Chen, Rui Hu, Sergio Casas, and Raquel Urtasun. PnPNet: End-to-End Perception and Prediction with Tracking in the Loop. In *CVPR*, pages 11553–11562, 2020. 3, 6
- [27] Bencheng Liao, Shaoyu Chen, Xinggang Wang, Tianheng Cheng, Qian Zhang, Wenyu Liu, and Chang Huang. MapTR: Structured Modeling and Learning for Online Vectorized HD Map Construction. In *ICLR*, 2023. 2
- [28] Bencheng Liao, Shaoyu Chen, Yunchi Zhang, Bo Jiang, Qian Zhang, Wenyu Liu, Chang Huang, and Xinggang Wang. MapTRv2: An End-to-End Framework for Online Vectorized HD Map Construction. *IJCV*, pages 1–23, 2024. 2

- [29] Xuewu Lin, Tianwei Lin, Zixiang Pei, Lichao Huang, and Zhizhong Su. Sparse4D: Multi-view 3D Object Detection with Sparse Spatial-Temporal Fusion. *arXiv preprint arXiv:2211.10581*, 2022. 2
- [30] Xuewu Lin, Zixiang Pei, Tianwei Lin, Lichao Huang, and Zhizhong Su. Sparse4D v3: Advancing End-to-End 3D Detection and Tracking. *arXiv preprint arXiv:2311.11722*, 2023. 1
- [31] Yingfei Liu, Tiancai Wang, Xiangyu Zhang, and Jian Sun. PETR: Position Embedding Transformation for Multi-view 3D Object Detection. In *ECCV*, pages 531–548, 2022. 2
- [32] Yingfei Liu, Junjie Yan, Fan Jia, Shuailin Li, Aqi Gao, Tiancai Wang, and Xiangyu Zhang. PETRv2: A Unified Framework for 3D Perception from Multi-Camera Images. In *ICCV*, pages 3262–3272, 2023. 2
- [33] Scott M Lundberg and Su-In Lee. A Unified Approach to Interpreting Model Predictions. In *NeurIPS*, pages 4765–4774. Curran Associates, Inc., 2017. 1
- [34] Wenjie Luo, Bin Yang, and Raquel Urtasun. Fast and Furious: Real Time End-to-End 3D Detection, Tracking and Motion Forecasting with a Single Convolutional Net. In *CVPR*, pages 3569–3577, 2018. 3
- [35] Tim Meinhardt, Alexander Kirillov, Laura Leal-Taixe, and Christoph Feichtenhofer. TrackFormer: Multi-Object Tracking with Transformers. In *CVPR*, pages 8844–8854, 2022. 2, 3
- [36] Jiquan Ngiam, Benjamin Caine, Vijay Vasudevan, Zhengdong Zhang, Hao-Tien Lewis Chiang, Jeffrey Ling, Rebecca Roelofs, Alex Bewley, Chenxi Liu, Ashish Venugopal, et al. Scene Transformer: A unified architecture for predicting future trajectories of multiple agents. In *ICLR*, 2022. 2
- [37] Bowen Pan, Jiankai Sun, Ho Yin Tiga Leung, Alex Andonian, and Bolei Zhou. Cross-view Semantic Segmentation for Sensing Surroundings. *IEEE Robotics and Automation Letters*, 5(3):4867–4873, 2020. 6
- [38] Chenbin Pan, Burhaneddin Yaman, Senem Velipasalar, and Liu Ren. CLIP-BEVFormer: Enhancing Multi-View Image-Based BEV Detector with Ground Truth Flow. In *CVPR*, pages 15216–15225, 2024. 2
- [39] Jonah Philion and Sanja Fidler. Lift, Splat, Shoot: Encoding Images from Arbitrary Camera Rigs by Implicitly Unprojecting to 3D. In *ECCV*, pages 194–210, 2020. 2, 6
- [40] Aditya Prakash, Kashyap Chitta, and Andreas Geiger. Multi-Modal Fusion Transformer for End-to-End Autonomous Driving. In *CVPR*, pages 7077–7087, 2021. 3
- [41] Shaoshuai Shi, Li Jiang, Dengxin Dai, and Bernt Schiele. Motion Transformer with Global Intention Localization and Local Movement Refinement. *NeurIPS*, 35:6531–6543, 2022. 2
- [42] Sebastian Thrun, Wolfram Burgard, and Dieter Fox. *Probabilistic Robotics*. MIT Press, 2005. 4
- [43] A Vaswani. Attention Is All You Need. In *NeurIPS*, 2017. 2, 4
- [44] Royden Wagner, Ömer Şahin Taş, Marvin Klemp, Carlos Fernandez, and Christoph Stiller. RedMotion: Motion Prediction via Redundancy Reduction. *Transactions on Machine Learning Research*, 2024. 2
- [45] Shihao Wang, Yingfei Liu, Tiancai Wang, Ying Li, and Xiangyu Zhang. Exploring Object-Centric Temporal Modeling for Efficient Multi-View 3D Object Detection. In *ICCV*, pages 3621–3631, 2023. 2
- [46] Yue Wang, Vitor Campagnolo Guizilini, Tianyuan Zhang, Yilun Wang, Hang Zhao, and Justin Solomon. DETR3D: 3D Object Detection from Multi-view Images via 3D-to-2D Queries. In *CoRL*, pages 180–191, 2022. 2
- [47] Xinhua Weng, Ye Yuan, and Kris Kitani. PTP: Parallelized Tracking and Prediction with Graph Neural Networks and Diversity Sampling. *IEEE Robotics and Automation Letters*, 6(3):4640–4647, 2021. 3
- [48] Xinhua Weng, Boris Ivanovic, Yan Wang, Yue Wang, and Marco Pavone. PARA-Drive: Parallelized Architecture for Real-time Autonomous Driving. In *CVPR*, pages 15449–15458, 2024. 2, 3, 6, 7
- [49] Chenyu Yang, Yuntao Chen, Hao Tian, Chenxin Tao, Xizhou Zhu, Zhaoxiang Zhang, Gao Huang, Hongyang Li, Yu Qiao, Lewei Lu, et al. BEVFormer v2: Adapting Modern Image Backbones to Bird’s-Eye-View Recognition via Perspective Supervision. In *CVPR*, pages 17830–17839, 2023. 2
- [50] Fangao Zeng, Bin Dong, Yuang Zhang, Tiancai Wang, Xiangyu Zhang, and Yichen Wei. MOTR: End-to-End Multiple-Object Tracking with Transformer. In *ECCV*, pages 659–675, 2022. 2, 3, 5
- [51] Wenyuan Zeng, Wenjie Luo, Simon Suo, Abbas Sadat, Bin Yang, Sergio Casas, and Raquel Urtasun. End-to-end Interpretable Neural Motion Planner. In *CVPR*, pages 8660–8669, 2019. 2, 3
- [52] Jiang-Tian Zhai, Ze Feng, Jinhao Du, Yongqiang Mao, Jiang-Jiang Liu, Zichang Tan, Yifu Zhang, Xiaoqing Ye, and Jingdong Wang. Rethinking the Open-Loop Evaluation of End-to-End Autonomous Driving in nuScenes. *arXiv preprint arXiv:2305.10430*, 2023. 3, 7
- [53] Lu Zhang, Peiliang Li, Sikang Liu, and Shaojie Shen. SIMPL: A Simple and Efficient Multi-agent Motion Prediction Baseline for Autonomous Driving. *IEEE Robotics and Automation Letters*, 2024. 2
- [54] Tianyuan Zhang, Xuanyao Chen, Yue Wang, Yilun Wang, and Hang Zhao. MUTR3D: A Multi-camera Tracking Framework via 3D-to-2D Queries. In *CVPR*, pages 4537–4546, 2022. 6, 1
- [55] Wenzhao Zheng, Ruiqi Song, Xianda Guo, Chenming Zhang, and Long Chen. GenAD: Generative End-to-End Autonomous Driving. In *ECCV*, pages 87–104, 2025. 1, 2, 3, 4, 6, 7
- [56] Zikang Zhou, Luyao Ye, Jianping Wang, Kui Wu, and Kejie Lu. HiVT: Hierarchical Vector Transformer for Multi-Agent Motion Prediction. In *CVPR*, pages 8823–8833, 2022. 2

# Divide and Merge: Motion and Semantic Learning in End-to-End Autonomous Driving

## Supplementary Material

### 6. Tracking as a Semantic Task

We justify the similarity of detection and tracking on nuScenes [3] by analyzing the information learned by the object query. E2E detection and tracking models decode each query into category, location, size, orientation, and velocity of the object. The category is clearly a semantic attribute, while location, size, and orientation serve as spatial complements to the category, all being time-invariant. In contrast, velocity is derived from time, making it a motion attribute. However, measuring velocities is not a common practice in detection, but required by the nuScenes benchmark. Therefore, detection models trained on nuScenes are able to perform tracking without any additional learning effort assuming constant velocity motion [19, 21, 30, 54]. Given that current modular E2E models are all trained on nuScenes, we regard the tracking component in these methods closely resembles detection, where learning semantics is dominating.

### 7. SHAP Values

We use SHAP values [33] to inspect the negative transfer in detection and tracking. SHAP values quantify the contribution of each feature to the change in a model’s output, offering insights into the reasoning behind machine learning model inferences. We visualize the SHAP values of 256 features of the object query with respect to the object classification output to interpret the negative transfer in UniAD [21] and to demonstrate how our method effectively mitigates this issue. Figure 6a compares the SHAP values between stage 1 and stage 2 of UniAD, sorted in descending order. The left half of the difference bar chart predominantly displays negative values, while the right half shows positive values, indicating that the SHAP values in stage 1 are more uniformly distributed, while ones in stage 2 are more concentrated. Compared with a flat distribution, the concentration means that less features are useful to the classification task, therefore reduces the detection and tracking performance. This observation aligns with our argument that during the second stage, object queries are expected to learn motion information, which fails to contribute to the perception task. Specifically, the velocity learned in stage 1 is sufficient for tracking (predicting the next timestep), while insufficient for the long-term prediction in 12 timesteps (6 seconds). Therefore, the object query is forced to learn more motion states which are ambiguous to identify objects, interfering with the space for semantic

information. In contrast, the SHAP values in DMAD maintain a similar distribution across both stages, as shown in Fig. 6b.

### 8. Queue Length

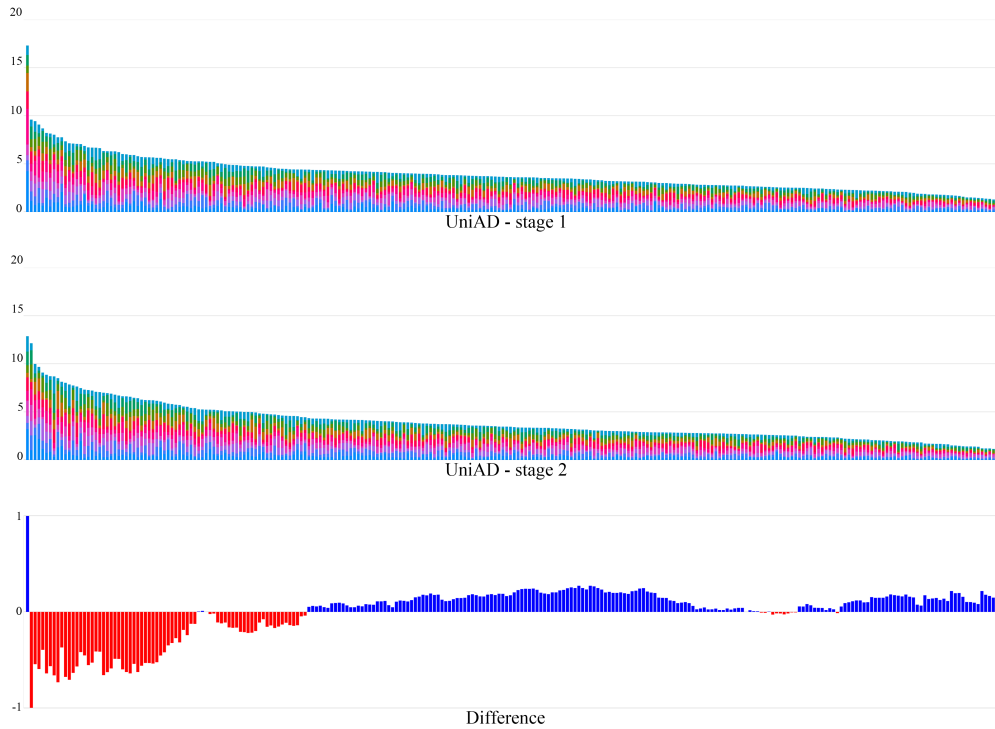
We adopt a different queue length configuration from that of the original UniAD. As mentioned in Sec. 4.1, the rationale behind our decision is that reducing the queue length in stage 2 affects the performance, hindering the observation of negative transfer. Table 7 shows an ablation study of queue length on UniAD, presenting the performance drops by reduced queue length. As the training time scales almost linearly to the queue length, we opt for a queue length of 3 to reduce training time of each iteration.

### 9. Effect of Unimodal Prediction Horizon

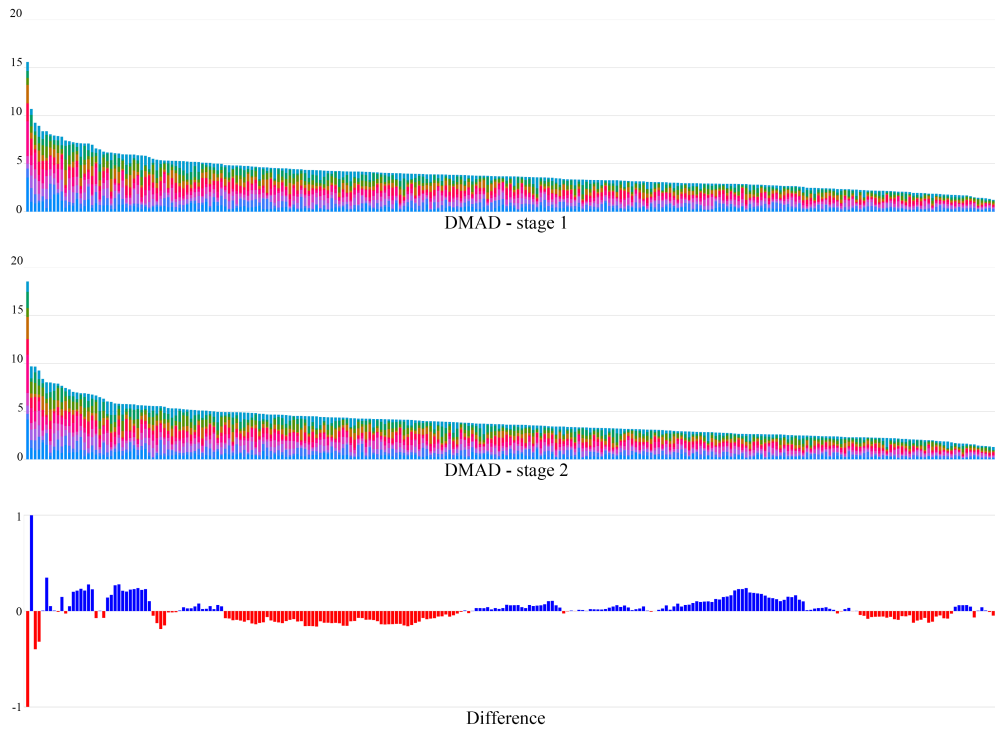
We conduct experiments on the number of future steps in unimodal prediction, as shown in Tab. 8. We observe that the unimodal prediction horizon influences the proportion of motion information within the BEV feature, thereby impacting the performance of both semantic and motion tasks. A long prediction horizon degrades the performance of semantic tasks, as the BEV feature is forced to prioritize motion learning in order to predict distant future outcomes. Experiments show that a prediction horizon of 6 seconds minimizes the collision rates, but performs worst in tracking. Although this phenomenon can also be referred to as negative transfer, our approach is unable to address this specific type, as the BEV feature is shared across all tasks and is expected to encapsulate both types of information. To balance motion and semantic information within the BEV feature, we set the prediction horizon to 4 seconds.

### 10. Visualizations of Reducing Collisions Rates

We provide qualitative comparisons between DMAD and UniAD in Fig. 7, showcasing how the improved perception and prediction reduces collision rates.



(a) SHAP values of UniAD



(b) SHAP values of DMAD

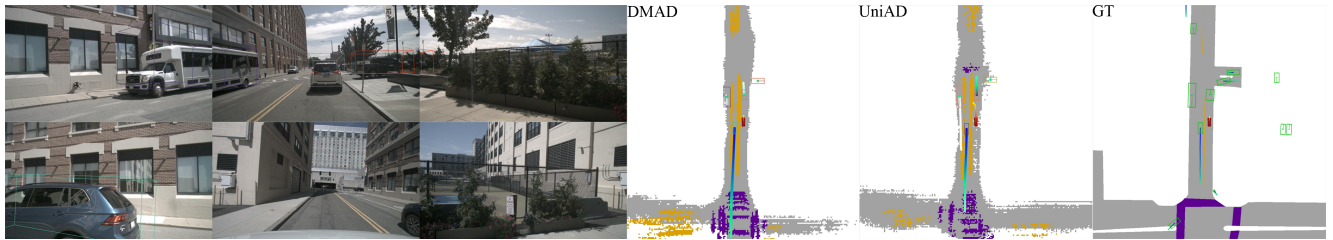
Figure 6. **SHAP values visualization.** Each colorful bar represents the SHAP values of a single feature with respect to different classes (coded by colors). The object query consists of 256 features, forming 256 bars in each chart. The difference is computed as stage 1 minus stage 2, aggregating all classes, where red indicates a negative value and blue signifies a positive value.

Queue length stage 1	Queue length stage 2	NDS $\uparrow$	mAP $\uparrow$	AMOTA $\uparrow$	AMOTP $\downarrow$	IDS $\downarrow$	Lanes $\uparrow$	Drivable $\uparrow$	EPA $\uparrow$	minADE $\downarrow$	Avg. L2 $\downarrow$	Avg. Col. $\downarrow$
3	3	0.491	0.377	0.354	1.34	1381	0.312	0.678	<b>0.495</b>	0.692	0.784	0.150
5	3	0.499	0.381	0.362	1.34	956	0.313	<b>0.692</b>	0.492	<b>0.655</b>	0.656	0.130
5	5	<b>0.501</b>	<b>0.384</b>	<b>0.370</b>	<b>1.32</b>	<b>885</b>	<b>0.314</b>	0.690	<b>0.495</b>	0.714	<b>0.615</b>	<b>0.123</b>

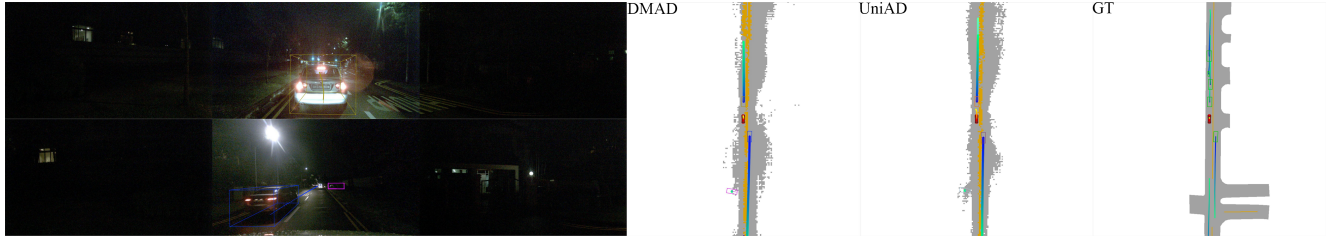
Table 7. Effect of queue length on UniAD.

Unimodal pred. horizon	NDS $\uparrow$	mAP $\uparrow$	AMOTA $\uparrow$	AMOTP $\downarrow$	IDS $\downarrow$	Lanes $\uparrow$	Drivable $\uparrow$	EPA $\uparrow$	minADE $\downarrow$	Avg. L2 $\downarrow$	Avg. Col. $\downarrow$
2s	<b>0.516</b>	<b>0.404</b>	<b>0.400</b>	<b>1.30</b>	<b>695</b>	0.321	0.691	0.534	0.735	0.679	0.220
4s	0.506	0.396	0.393	<b>1.30</b>	767	0.321	0.691	<b>0.535</b>	<b>0.723</b>	<b>0.625</b>	0.127
6s	0.504	0.396	0.384	<b>1.30</b>	751	<b>0.322</b>	<b>0.700</b>	0.525	0.743	0.629	<b>0.117</b>

Table 8. Effect of unimodal prediction horizon on DMAD.



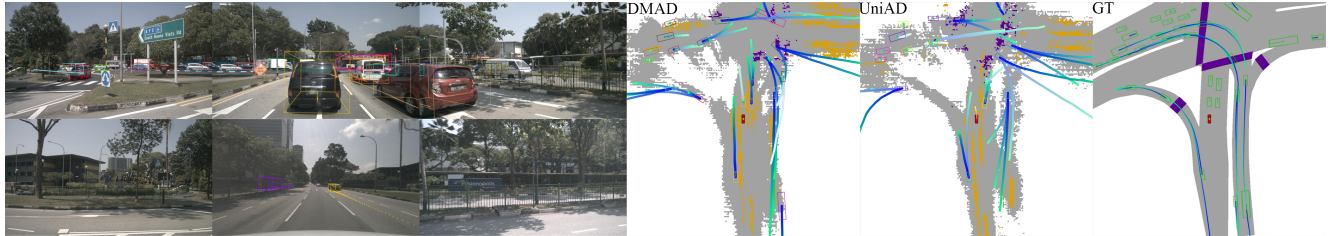
(a) The collision of UniAD is because of an inaccurate prediction of the lead vehicle.



(b) Both models make inaccurate predictions of the lead vehicle during the night. However, UniAD collides with the lead vehicle due to its aggressive driving policy.



(c) An inaccurate detection (the detected position is too close to the ego-vehicle) causes yielding, and then colliding with another vehicle.



(d) UniAD fails to detect the lead vehicle and collides with it.

Figure 7. Qualitative comparison between DMAD and UniAD. Each subfigure demonstrates a sample where UniAD encounters collision while DMAD does not.